Chapter 5

Applications of PISA-QMS

5.1 Transmission efficiency in RF-QMF

The distortion of the electric fields at the entrance region of the four rod electrodes is one of serious problems of RF-QMF, since it can lead to transmission loss of ions[9]. Hennequin and Inglebert[45,46] reported that the effective transmission efficiency in the fringing field was about 50% based on experiment. To minimize this fringing field effect on the transmission loss, several measures have been adopted. Brubaker[47] proposed addition of supplementary electrodes to which only an RF voltage was applied. Another way reported by Brubaker and Tuul[48] used an electrode shaped as a nozzle at the entrance to increase the acceleration voltage of ions. These measures, however, required substantial change in the design and cost, but RF-QMF remained at low cost-performance ratios.

We have examined the effect of the fringing field on the transmission efficiency in RF-QMF by simulating ion trajectories with our program PISA-QMS in order to enhance the transmission efficiency at the entrance part.

5.1.1 Ion injection with low energy

A schematic view of the entrance part of RF-QMF is shown in Fig.5-1. An ion beam is injected into the quadrupole electric field through an aperture on the shield case at the ground potential. This ion beam is focused around the closer end of the electrodes.

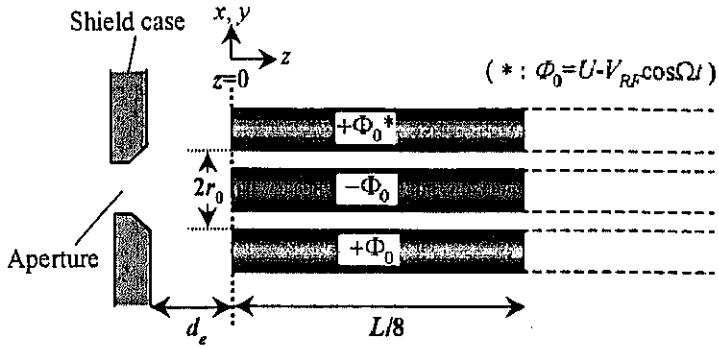

Fig.5-1 Schematic view of the entrance part of RF-QMF. The ion beam is injected into the the entrance part through the aperture of the grounded shield case, being focused around the end of the rod electrodes. The origin of the z coordinate is set at the end of the rod electrodes and d_e denotes the distance between the rods and the shield case.

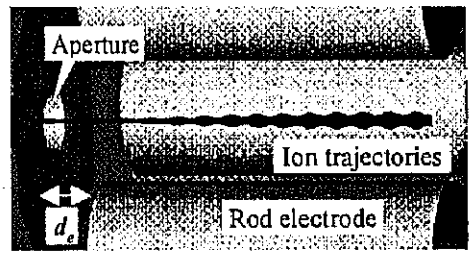

(a) Trajectories of the 85 u ions when a_x and q_x values were 0.2363 and 0.706, respectively.

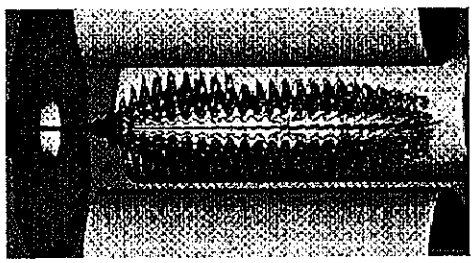

(b) Trajectories of the 300 u ions when a_x and q_x values were 0.2363 and 0.706, respectively.

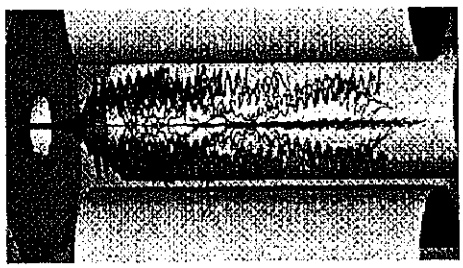

(c) Trajectories of the 500 u ions when a_x and q_x values were 0.2363 and 0.706, respectively.

Fig.5-2 Calculated trajectories of ions injected from the aperture of the shield case at an injection energy of 5 eV. The RF frequency and the focusing position were 2.1MHz and z=0.

At first, we calculated trajectories assuming that the ions with masses of 85u, 300u and 500u are focused on the closer end of the electrodes (z=0 in Fig.5-1). Usually, ions are injected into the entrance part of RF-QMF with an energy of 10-20eV. Here, in order to clarify the influence of the fringing field, a low injection energy of 5 eV was set for all three ion species. As seen in Fig.5-2, the trajectories of 85u ions converge well, so that all of the ions are transmitted. On the contrary, the trajectories of 300u and 500u ions have large transverse amplitudes of oscillations. Some of these ions cannot pass through RF-QMF. This is mainly due to the fact that the velocities of 300u and 500u ions across the fringing field are slow in comparison with the velocity of 85u ions.

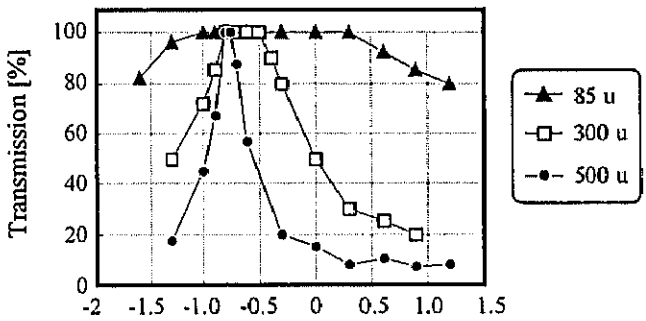

Fig.5-3 The dependence of transmission efficiencies on the position of the focal position.

Next, the dependence of the transmission efficiency on the different focal positions of ions was investigated with simulations. The calculated transmission efficiency is plotted as a function of normalized distance z/d_e in Fig.5-3. The origin of z coordinate is taken to be at the closer end of the four rod electrodes, while the distance between this end of the rods to the aperture is defined by d_e. The transmission efficiency of 85u ions is 100 % for focal positions in the range of $-1.0 \leq z/d_e \leq 0.3$. It is also 100 % for 300u ions, although the range of focal positions becomes as narrow as $-0.7 \leq z/d_e \leq 0.5$. For 500u ions, focal positions to give 100 % transmission are limited

in a very narrow range at around $z/d_e \approx -0.7$. Therefore, if we adjust the voltage applied to the focusing lens in such a way that the ion beam with the heaviest mass in the mass range of interest is focused onto the optimum position, the transmission efficiency of ions with lower masses are all 100 %. In practice, the adjustment of the voltages applied to the focusing lens is commonly carried out to obtain high transmission efficiencies. This confirms that there actually exists an optimal region of the focusing point.

We should note here the size of the focus and the transverse displacement of the focus from the center. The effect of the fringing field is indeed inevitable. The central region of a two-dimensional quadrupole field is a force-free region for ions. If ions are focused in a small region near z axis with small transverse momentum, ions would pass through the fringing field with the least transverse divergence. By the simulation results we clarified the actual region for ions to be converged near z axis. Therefore, high transmission efficiencies are expected if the ion beam is converged in that region by adding new focusing electrodes around the region as well as adjustment of the focusing voltage. Thus, a new design for the focusing lens or a new entrance structure for RF-QMF are obtained from PISA-QMS simulations.

5.1.2 Ion injection with high energy

To lower the dependence of the transmission efficiency on the ion mass number as was shown in Fig.5-3, ions are usually injected with a higher energy of 100-200 eV. A schematic view of the entrance part of RF-QMF in the case of the ion injection with higher energy is shown in Fig.5-4. The ions, however, need to be decelerated to 5-10eV before entering the space between the rod electrodes to avoid the decrease of the mass resolution due to ions passing fast through RF-QMF. In most cases, the decelerating electric field is generated by applying the decelerating voltage $+V_{dec}$ to all rod electrodes other than the voltage of $\pm(U\text{-}V_{RF}\cos\Omega t)$.

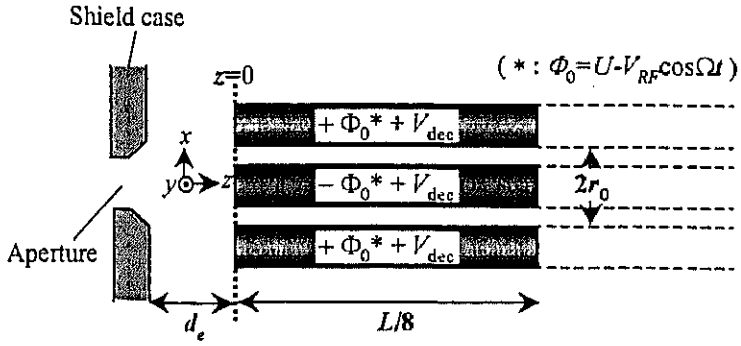

Fig.5-4 Schematic view of the entrance part of RF-QMF in the case of ion injection with a higher energy of 100-200eV. The injected ion beam is decelerated by applying $+V_{dec}$ to all four rod electrodes, being focused around the end of the rod electrodes. The origin of the z coordinate is set at the end of the rod electrodes and d_e denotes the distance between the rods and the shield case.

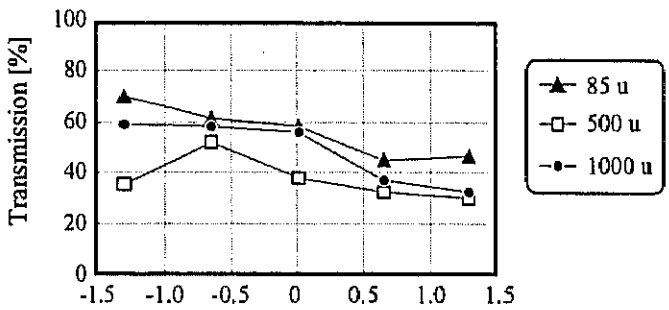

Fig.5-5 The dependence of transmission efficiencies on the position of the focal position when the ion injection energy and the decelerating voltage $+V_{dec}$ were set to be 135eV and 130V, respectively.

At first, we calculated the transmission efficiencies of the ions with masses of 85u, 500u and 1000u with varying the focal position when the ion injection energy and the decelerating voltage $+V_{dec}$ were set to be 135eV and 130V, respectively. The a_x, q_x parameters were same as the a_x, q_x values used in the case of Fig.5-3. The calculated transmission efficiency is plotted in Fig.5-5 as a function of the focal position. Even low mass ions of 85u cannot transmit with 100% efficiency. On the other hand, higher mass ions of 500u and 1000u transmit with almost same efficiencies as that of 85u ions. The dependence of the transmission efficiencies on the focal

position are not so strong as in the case of Fig.5-3. The highest efficiency is about 60% at around $z/d_e \approx -0.6$, independently of the ion mass. This result is much different from the case of low energy injection. To clarify how the ion transmission are determined in the case of higher energy injection, we investigated the transmission efficiencies with varying the a_x, q_x values when the focal point was fixed at z/d_e=-0.6. Fig.5-6 and Fig.5-7 show the dependence of the calculated transmission efficiencies on q_x values, when a_x=0.2363 and a_x=0.23, respectively. In the case of a_x=0.2363, the q_x value which gives the highest efficiencies among three ion species is lower than q_x=0.706, that is the q_x value of the tip of the stability region in Fig.3-5. For a_x=0.23, there is the q_x region in which the transmission efficiencies become 100%. This q_x region is assumed to be the actual stability region at the entrance part of RF-QMF. This actual stability q_x region at a_x=0.23 is narrower as the ion mass number is higher. This is mainly due to the difference of the velocities in decelerating field among the ion species. The actual stability q_x regions of all ion species are shifted to low q_x side. This shift of the stability region is understood as described below.

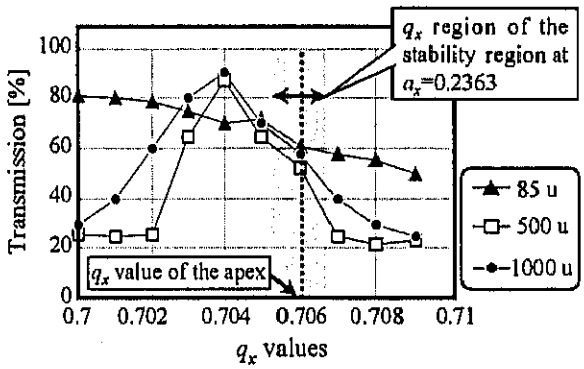

Fig.5-6 The dependence of transmission efficiencies on q_x (= $-q_y$) values in case of a_x=0.2363 (= $-a_y$).

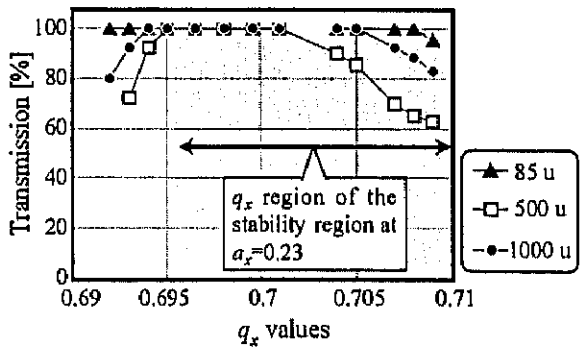

Fig.5-7 The dependence of transmission efficiencies on q_x (= $-q_y$) values in case of a_x=0.23 (= $-a_y$).

Since the decelerating voltage $+V_{dec}$ is applied to all four rod electrodes as shown in Fig.5-4, the total voltages on the two pairs of the electrodes placed on x-axis and y-axis are $+(U-V_{RF}\cos\Omega t) + V_{dec}$ and $-(U-V_{RF}\cos\Omega t) + V_{dec}$, respectively. The actual DC voltage U^* in x-direction

becomes $U+V_{dec}$, while U^* in y-direction is $U-V_{dec}$. In other words, the actual a_x^* values increase and the actual a_y^* values decrease in comparison with the theoretical a_x, a_y values in eqs.(3-2-7) and (3-2-8). According to the changes of these a_x^*, a_y^* values, the stability region is also assumed to be changed. The stability diagram around its tip is schematically shown in Fig.5-8. The theoretical stability region and the actual one are enclosed by broken lines and solid lines, respectively. The border line of the actual stability region in x-direction apparently is shifted to lower a_x side than that of the theoretical one because of $a_x<a_x^*$. On the other hand, the actual stability region in y-direction is shifted to higher a_y side because of $a_y>a_y^*$. Consequently, the practical stability region in both x- and y-directions at the entrance part of RF-QMF is shifted in the direction of $-q_y$ as shown in Fig.5-8. As ions traverse far from the fringing field, the stability region becomes close to the theoretical one. Therefore, ions which can actually transmitted are determined by the overlap of the stability regions in the whole structure of RF-QMF as indicated by the shaded region in Fig.5-8.

Thus, the shifted stability region at the entrance part of RF-QMF is clarified by applying PISA-QMS. The actual stability region for the whole structure of RF-QMF is also obtained. Operating RF-QMF based on this actual stability region is one of the measures to improve the mass resolution as well as the transmission efficiencies.

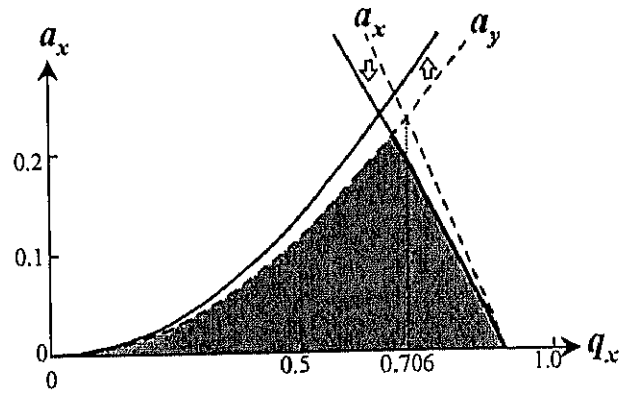

Fig.5-8 The schematic diagram of the practical stability region at the entrance part of RF-QMF when ions are injected with a higher energy of 100-200eV into the decelerating field.

5.2 Trapping efficiency of ions injected into ITMS

After the development of the mass-selective instability scanning operation by Stafford *et al.*[49], ITMS has come to be used in various fields by virtue of its versatility. In particular, techniques for injection of externally formed ions into ITMS have permitted extension of its applications to mass spectroscopy by using many kinds of ion sources. One serious problem, however, is the unequal sensitivity for different masses. This is mainly due to the fact that there is a difference in the trapping efficiency for the mass of injected ions.

The trapping efficiency of injected ions has been discussed by many authors from several view points. The dependence of the direction of injected ions was reported in refs.[50-53]. Ghosh and Arora[54] discussed the effect of the initial phase ϕ of the RF voltage of $V_{RF}\cos(\Omega t+\phi)$ applied to the ring electrode during the ion injection period (see also ref[53]). Louris *et al.*[40] and McLuckey *et al.*[55] examined the influence of the amplitude V_{RF} and the dependence of the parameter q_u in the Mathieu equation and the pressure of ion buffering gas. Schwartz *et al.*[56] studied the influence of kinetic energy of injected ions. As already explained in regard to the coefficients C_{2n} plotted in Fig.3-9 (see Subsection 3.3.3), the dominant mode of ion oscillations is a simple harmonic oscillation corresponding to n=0 at small values of q_z (see eq.(3.3.19)). When ions from an external ion source are injected into ITMS, the value of q_z is set small to confine the ions in a stable orbit in ITMS[54,57]. All the previous investigations, therefore, approximated ion motions as the n=0 oscillation only. In such a conventional approximation, optimum values like V_{RF} or ion injection energies to give the maximum trapping efficiency exhibited large discrepancies between theoretical predictions and experimental values[40]. The optimum values for the maximum trapping efficiency calculated from our PISA-QMS differed also from experiments. To remove this discrepancy, we have carried out further investigations on the mechanism of ion trapping in ITMS using PISA-QMS.

5.2.1 Inclusion of higher modes of oscillations

At first, the coefficients C_{2n} plotted in Fig.3-9 should be remembered. This plot indicates that C_{2n}'s are small for n=±2, but are appreciable for n=±1. The coefficient C_{2n} for n=-1 becomes substantially large as q_z goes to 0.9. In the present investigation, therefore, the second and third dominant oscillations were taken into account to describe the motions of injected ions even at sufficiently small q_z. Including the three modes of oscillations specified by n=0, n=-1 and n=+1, the motions of ions can be expressed in the form of

$$z(t) \approx A_{0z}\cos(\omega_0 t+\phi_0) - C_{-2}A_{0z}\cos(\omega_{-1}t+\phi_{-1}) - C_{+2}A_{0z}\cos(\omega_{+1}t+\phi_{+1})$$

$$= A_{0z}\cos(\omega_0 t+\phi_0) - C_{-2}A_{0z}\cos\{(\omega_0-\Omega)t+\phi_{-1}\} - C_{+2}A_{0z}\cos\{(\omega_0+\Omega)t+\phi_{+1}\}. \quad (5.2.1)$$

The kinetic energy of ions is given by

$$\text{K.E.} \approx \frac{1}{8}mA_{0z}{}^2\Omega^2\left\{\beta_z{}^2 + C_{-2}{}^2(\beta_z-2)^2 + C_{+2}{}^2(\beta_z+2)^2\right\}. \quad (5.2.2)$$

From eq.(3.3.16), the frequency of the second dominant oscillation (n=-1) is ω_0-Ω, and that of the third dominant oscillation (n=+1) is ω_0+Ω. In the following subsections, we discuss how these higher modes of oscillations play an important role in the ion trapping efficiency of ITMS.

5.2.2 The role of higher modes of oscillations

At first, we examined the motion of ions injected into ITMS using PISA-QMS. The ion mass was tentatively assumed to be 100u. The initial position of the ion at the time t=0 was taken to be $r(t=0)$=0 and $z(t=0)=0.95z_0=0.672r_0$ as indicated in Fig.5-9. Other parameters used in the simulation are listed in Table 5-1. Fig.5-10(a) shows the position of the 100u ion in z-direction as a function of time, simulated by PISA-QMS. The simulated velocity of the ion in-z direction is displayed in Fig.5-10(b). The q_z value was chosen to be 0.1. According to eq.(3.2.12), the value

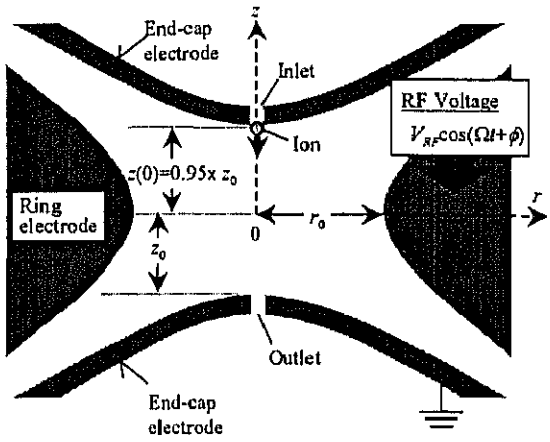

Fig.5-9 Cross section of ITMS. An ion is injected from the initial position ($r(0)$, $z(0)$)=(0, $0.95z_0$) with energy E.

Table 5-1 The ITMS parameters used to simulate the ion motion shown in Figs.5-5 and 5-6.

RF voltage $V_{RF}\cos(\Omega t+\phi)$	
RF frequency $f=\Omega/2\pi$	909kHz
RF amplitude V_{RF}	84.52V
Ion mass	100 u
Inner radius of the ring electrode r_0	10mm
q_z value (β_z value)	0.1 (0.06061)
Injection energy E	1eV
Helium gas pressure P_{He}	1.0×10^{-4} Torr (1.33×10^{-4} Pa)
Assumed radius of space charge R_s	5mm
Ion density ρ	1.9×10^{13} /mm³

of q_z =0.1 yields β_z=0.07085 with a_z =0. The motion of the injected 100u ion approximated by only the n=0 mode of oscillation is simply obtained from eq.(5.2.1) by substituting the values of β_z=0.07085 and C_{-2}= C_{+2}=0. This motion is also plotted in Fig.5-10(a). It is evident that the fundamental frequency of the oscillation in $z(t)$ obtained from the simulation is lower than $\omega_z/2\pi$ for the approximated motion including only the n=0 oscillation. The difference in the velocity obtained by the simulation from the approximated n=0 oscillation is more apparent as seen in Fig.5-10(b). The velocity dz/dt obtained from the simulation is modulated with higher frequency, whereas dz/dt for the n=0 oscillation only must be a smooth sine wave function.

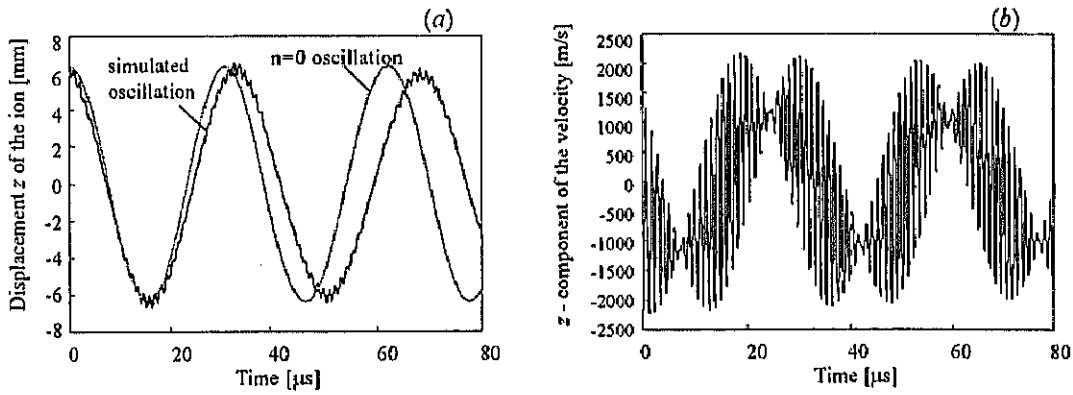

Fig.5-10 Simulation of the ion motion in ITMS. Simulated position of the 100 u ion in-z direction and its velocity in z-direction are shown in (*a*) and (*b*), respectively. The approximated n=0 oscillation (eq.(3.3.19)) is also plotted in (*a*).

Before discussing the role of the second and the third dominant oscillations, we should inspect the value of β_z. Fundamental angular frequencies $\omega_0^{(s)}$ were calculated by PISA-QMS under the condition of q_z<0.4. Then they were converted to $\beta_z^{(s)}$ according to $\omega_0^{(s)} = (\Omega/2)\beta_z^{(s)}$ analogous to eq.(3.3.20). The results are plotted in Fig.5-11 with open circles. The values of β_z calculated from eq.(3.2.12) are also shown in the same figure by the solid line. The values of $\beta_z^{(s)}$ are in good agreement with β_z in the range of q_z >0.25. At lower values of q_z, the values of $\beta_z^{(s)}$ are smaller than β_z. The decrease in $\beta_z^{(s)}$ from β_z becomes 10 % or more at q_z<0.1. This result may be ascribed to the fact that the collisions of ions with buffering gas atoms and the space charge effect are taken into account in PISA-QMS. In particular, the space charge mainly causes the decrease, because it acts as a Coulomb repulsive force, diminishing the trapping force. This is the decrease in restoring force in oscillations, and leads to the decrease in the frequency. By contrast, eq.(3.2.12) is an approximate formula for values of β_z, but it includes neither the collisions nor the space charge effect. The open circles in Fig.5-11 give us a realistic empirical relation of q_z *vs.* $\beta_z^{(s)}$. We use this empirical relation in the following discussions.

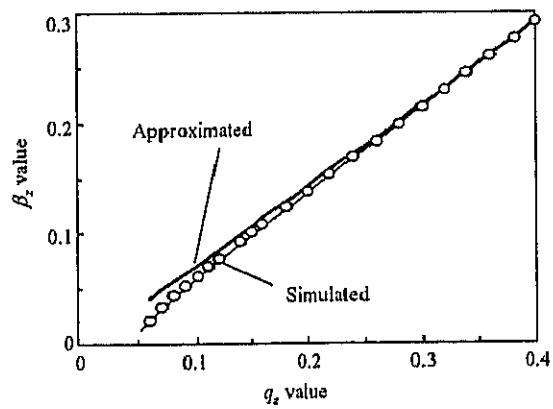

Fig.5-11 The relationship between q_z and β_z values. Open circles are obtained by the simulation. Theoretical approximation expressed in eq.(3.2.12) is drawn by the solid line.

According to the above empirical relation, we obtain $\beta_z^{(s)}$=0.06061 for q_z=0.1. With this $\beta_z^{(s)}$, ion trajectories were calculated for the following two cases.

Case 1. The ion trajectory is approximated with n=0 and n=-1 oscillations given by

$$z(t) \approx A_{0z}\cos(\omega_0 t+\phi_0) - C_{-2}A_{0z}\cos(\omega_{-1}t+\phi_{-1})$$

$$= A_{0z}\cos(\omega_0 t+\phi_0) - C_{-2}A_{0z}\cos\{(\omega_0-\Omega)t+\phi_{-1}\}. \qquad (5.2.3)$$

Case 2. The ion trajectory is approximated with n=0 and n=± 1 oscillations given by

$$z(t) \approx A_{0z}\cos(\omega_0 t+\phi_0) - C_{-2}A_{0z}\cos(\omega_{-1}t+\phi_{-1}) - C_{+2}A_{0z}\cos(\omega_{+1}t+\phi_{+1})$$

$$= A_{0z}\cos(\omega_0 t+\phi_0) - C_{-2}A_{0z}\cos\{(\omega_0-\Omega)t+\phi_{-1}\} - C_{+2}A_{0z}\cos\{(\omega_0+\Omega)t+\phi_{+1}\}. \qquad (5.2.4)$$

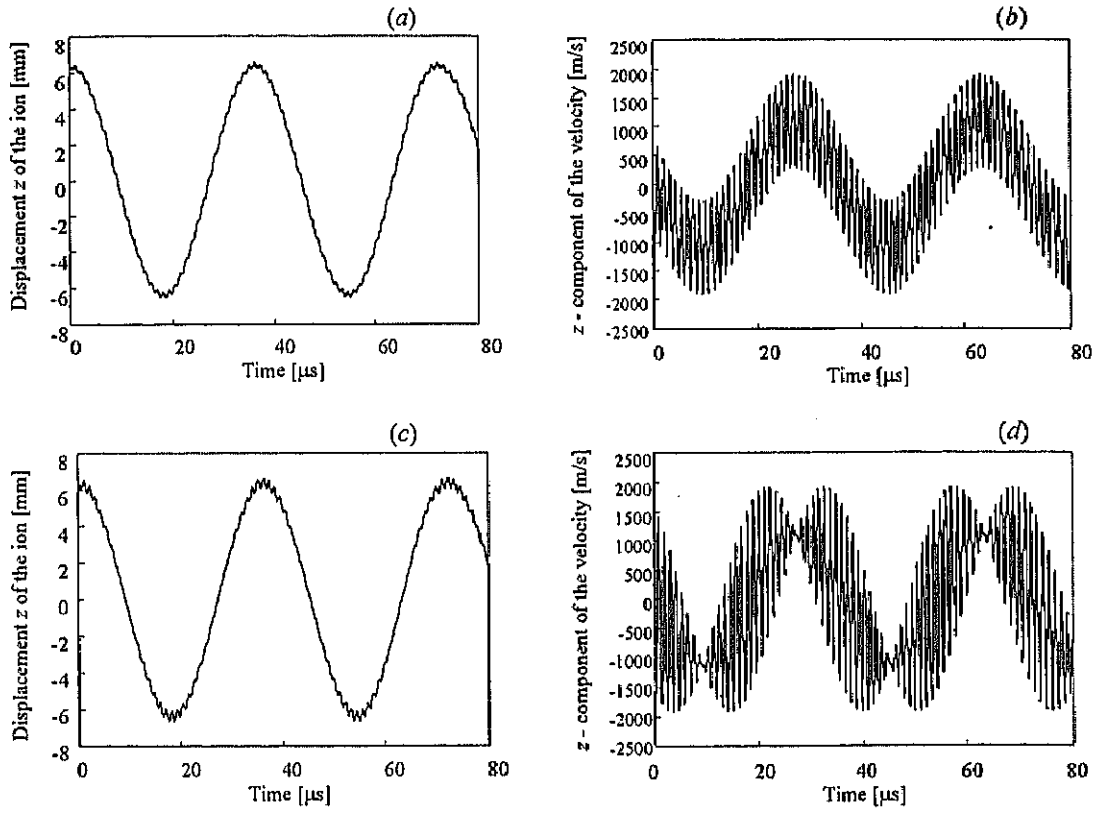

Fig.5-12 Ion trajectories and velocities in ITMS. Ion trajectory in (*a*) and velocity in (*b*) are obtained when ion motion is approximated with the combination of n=0 and -1 oscillation modes. Ion trajectory in (*c*) and velocity in (*d*) are obtained when ion motion is approximated with the combination of n=0 and ± 1 oscillation modes.

The ion trajectories calculated from the above equations under the conditions of ϕ_0=0, and ϕ_{-1} =ϕ_{+1}=1.1π are shown in Figs.5-12(a) and (c) for cases 1 and 2, respectively. These trajectories are very similar to the trajectory obtained from the simulation shown in Fig.5-10(a). The ion velocities calculated in a similar manner as the trajectories are presented in Figs.5-12(b) and (d). The velocity of case 1 is quite different from that obtained from the simulation. However, the velocity of case 2 is surprisingly similar to the simulation. Thus, we verified that the second and third dominant modes of oscillations play a crucial role in the approximation of the motion of injected ions with low q_z values.

5.2.3 Initial phase of RF voltage and ion trapping probability

In ITMS equipped with an external ion source, ions are injected from the inlet of the end-cap electrode at various RF phase ϕ of the voltage $V_{RF}\cos(\Omega t+ \phi)$. We assume the distribution of ions is uniform over the RF phase angle of ϕ =2π. The spatial distribution of ions at the inlet is also assumed to be uniform. The ion trapping efficiency is defined by

$$T = \frac{1}{2\pi}\int_0^{2\pi} P(\phi)d\phi\,, \tag{5.2.5}$$

where $P(\phi)$ stands for the probability of ion trapping at an RF phase ϕ.

At first, the trapping probability was examined. When the motion of injected ions is approximated only by the fundamental oscillation mode (n=0 mode) as in previous works, the relationship between the injection energy E and the amplitude A_0 is given by

$$A_0 = \sqrt{\frac{2e_0E}{m(1+\omega_0{}^2)} + z_0{}^2}\,, \tag{5.2.6}$$

with initial conditions of $z(t=0) \approx z_0$ and $(dz/dt)_{t=0} = -\sqrt{2e_0E/m}$. In this case, the amplitude A_0 is always greater than z_0, and independent of the RF phase ϕ_0. This implies that ions cannot remain in ITMS.

We investigated how the trapping probability depends on the RF phase ϕ using our PISA-QMS. Ion trajectories were calculated on the assumption that 1000 ions were injected from the inlet of one end-cap electrode at various RF phase ϕ. The initial position of 1000 ions was taken to be $z(t=0)=0.95z_0$ as shown in Fig.5-9. Other parameters used were as listed in Table 5-2. The ions were defined as being trapped, if they were oscillating with amplitudes $A_0 \leq z_0$ for 100 μs after their injection.

Table 5-2 The ITMS parameters used to simulate the ion motions shown in Figs.5-8 and 5-9.

RF voltage $V_{RF}\cos(\Omega t+\phi)$	
RF frequency $f=\Omega/2\pi$	909kHz
RF amplitude V_{RF}	84.52V
Ion mass	100 u
Inner radius of the ring electrode r_0	10mm
q_z value (β_z value)	0.1 (0.06061)
Injection energy E	2eV
Helium gas pressure P_{He}	1x10^{-4}Torr (0.133 Pa)
Assumed radius of space charge R_s	5mm
Ion density ρ	1.9 X 10^{3} /mm^{3}

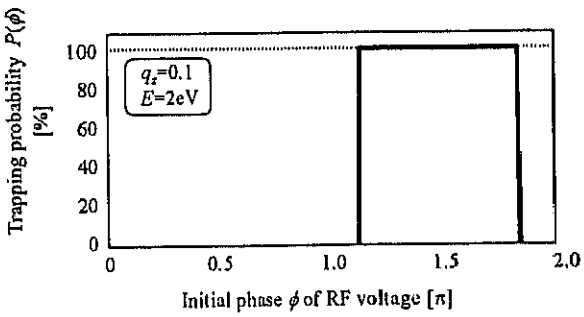

Fig.5-13 Simulated trapping probability $P(\phi)$ vs. the initial phase ϕ of the RF voltage under conditions of E=2eV, q_z=0.1.

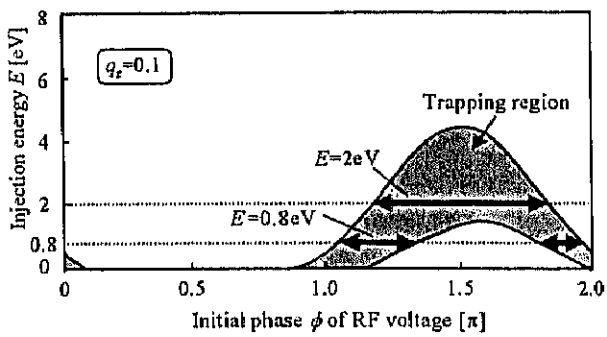

Fig.5-14 Simulated trapping region in E, ϕ space for q_z=0.1.

Fig.5-13 shows the probability $P(\phi)$ for ions injected at an energy of 2eV as a function of the RF phase ϕ. The value of q_z was assumed to be 0.1. Contrary to the prediction of the approximation in the n=0 mode oscillation only, ions injected in the RF phase from ϕ=1.16π to ϕ=1.84π are trapped with the probability of 100 %. Ions injected in other RF phases are never trapped, namely $P(\phi)$=0%. If we inject ions at a lower energy, at 0.8eV for example, the range of the RF phase giving 100 % probabilities splits into two narrow ranges of 1.03 $\pi \leq \phi \leq$ 1.34π and 1.8 $\pi \leq \phi \leq$ 1.96π. At injection energies higher than 4.5 eV, ions are not trapped in the whole range of the RF phase of 2π. The shaded area in Fig.5-14 represents the 100 % trapping region in the E-ϕ plane. Thus, it is evident from our simulation that the ion trapping probability depends on the RF phase, the injection energy and the value of q_z.

The results of our simulation presented above are also reproduced in fairly good approximation in terms of the sine wave functions including the second and third dominant oscillations. If we approximate the motions of injected ions to the function defined by eq.(5.2.6), the amplitude of ion oscillations is expressed as follows:

$$A_0 = \frac{-b \pm \sqrt{b^2 - ac}}{a}, \tag{5.2.7}$$

with

$$a = \omega_0^2 \left\{ (C_{-2} + C_{+2})^2 \cos^2 \phi_1 - 1 \right\} + (C_{-2}\omega_{-1} + C_{+2}\omega_{+2})^2 \sin^2 \phi_1$$

$$b = \omega_0^2 z_0 (C_{-2} + C_{+2}) \cos \phi_1 + \sqrt{\frac{2e_0 E}{m}} (C_{-2}\omega_{-1} + C_{+2}\omega_{+2}) \sin \phi_1$$

$$c = \omega_0^2 z_0^2 + \frac{2e_0 E}{m} \tag{5.2.8}$$

The amplitudes A_0 calculated from eqs.(5.2.7) with (5.2.8) at injection energies of 0.8 and 2 eV are represented in Figs.5-15(a) and (b), respectively.

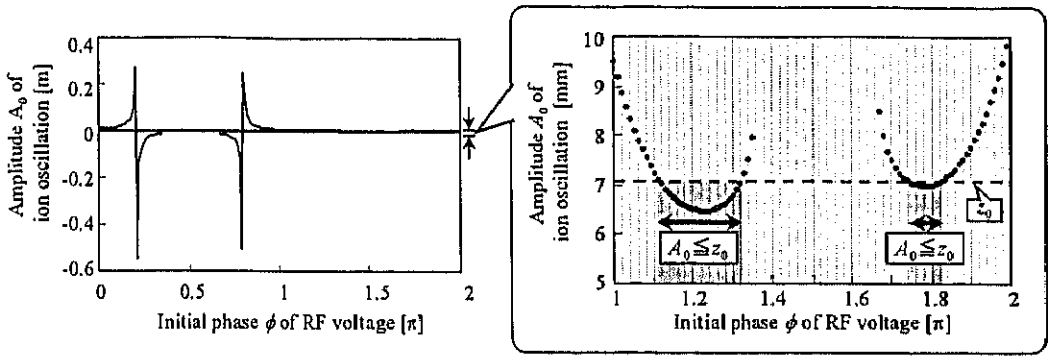

Fig.5-15(a) Simulated amplitude A_0 of ion oscillation under the conditions of E=0.8eV, q_z=0.1.

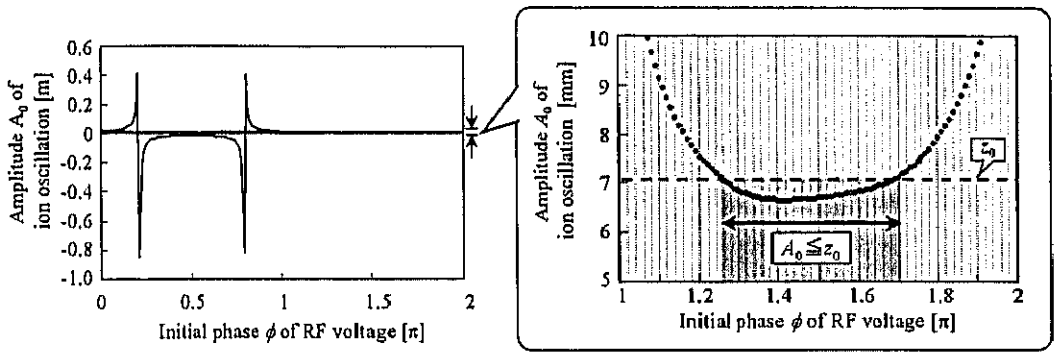

Fig.5-15(b) Simulated amplitude A_0 of ion oscillation under the conditions of E=2eV, q_z=0.1.

The value of q_z was assumed to be 0.1 in both cases. There are regions of RF phase ϕ where the amplitude A_0 becomes equal to or lower than z_0. This means that ions injected in those RF phases are trapped in ITMS. The explicit numerical values of those RF phase regions are $1.12\pi \leq \phi \leq 1.32\pi$ and $1.74\pi \leq \phi \leq 1.82\pi$ at the injection energy of 0.8 eV. The RF phase ϕ at another injection energy of 2 eV is limited within $1.26\pi \leq \phi \leq 1.69\pi$. These values of phase regions are very close to those obtained from the simulation. The trapping RF phases obtained from the simulation are slightly wider than the results of the approximate calculation with eqs.(5.2.7) and (5.2.8). This is due to the inclusion of collisions of ions with helium buffering gas in our simulation program PISA-QMS. In this manner, we proved using the program PISA-QMS that the function composing the fundamental, second and third dominant modes of oscillations of

ions gives us a fairly good approximation to analyze the dependence of the RF phase on the ion trapping probability.

5.2.4 Injection energies and ion trapping efficiency

The trapping efficiency defined by eq.(5.2.5) was calculated using our simulation program PISA-QMS. The dependence of ion injection energies on the trapping efficiency T is shown in Fig.5-16 for several q_z values from 0.1 to 0.3. The ordinate of this graph is proportional to the numerator of eq.(5.2.5) evaluated for infinitesimal energy increase dE. Explicitly it is written as

$$T(E)dE = \frac{1}{2\pi}\left\{\int_0^{2\pi} P(E,\phi)d\phi\right\}dE\,. \tag{5.2.9}$$

The pattern of the curve in Fig.5.16 can be understood to be the projection of the $T(E)dE$ onto the axis of E in Fig.5-14. The trapping efficiencies in Fig.5-16 exhibit a sharp maximum at a definite value of E for each q_z value. We define these values as *optimum* injection energy $E^{(s)}$. An empirical relation between $E^{(s)}$ and the corresponding q_z is plotted by black circles in Fig.5-17.

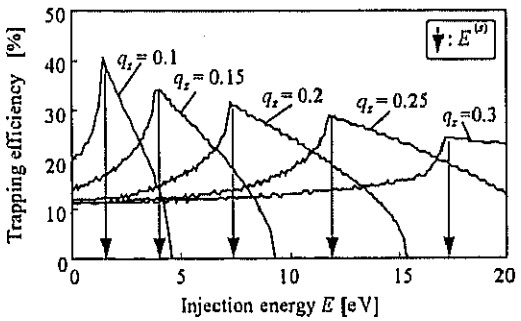

Fig.5-16 Injection energy dependence of the average trapping efficiencies obtained by simulation in the cases of q_z=0.1 - 0.3. For each case there is an optimum injection energy $E^{(s)}$ which gives maximum trapping efficiency.

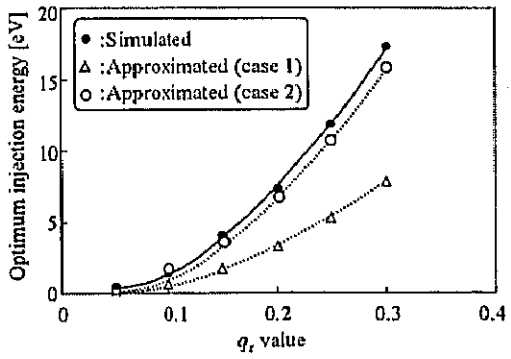

Fig.5-17 The simulated optimum injection energy versus q_z values in comparison with the maximum energy obtained by approximating ion motion in two cases: case 1, approximated with n=0 oscillation; case 2, approximated with n=0, ±1 oscillations.

On the other hand, maximum energies E_{max} of ion oscillations can be estimated by setting A_0 to $z(t=0)$ in the approximated sine wave functions. The results of calculations are plotted by open circles in Fig.5-17. The approximation including $n=0$ and $n=\pm 1$ modes of oscillations yields slightly smaller values of E_{max} than $E^{(s)}$. The values of E_{max} calculated with the approximation of the $n=0$ mode only are far below the values of $E^{(s)}$. This is the third example showing that the inclusion of the second and third dominant modes of oscillations with the $n=0$ mode oscillation is necessary for advanced discussions on the ion trapping efficiency in terms of approximated functions.

5.2.5 RF peak voltage and ion trapping efficiency

In practical operation of ITMS, ions from an ion source are injected for a certain period of time. This is called the ion injection period. The injection energy may be variable, but it is usually maintained at a definite value during the ion injection period. Once the injection energy is set, the trapping efficiency is a function of the mass of ions and RF voltage V_{RF} through q_z (see eq.(3.3.14b)). This can be understood from Fig.5-16 also. If we set an injection energy of 5 eV, the trapping efficiency increases from $q_z=0.3$ to $q_z \approx 0.15$, but it would drop to $T=0$ at a certain value in the range of $0.1 \leq q_z \leq 0.15$. The value of q_z is proportional to V_{RF}, so that the variation of the trapping efficiency with q_z can be regarded as V_{RF} dependence of the trapping efficiency, if we take only one mass m.

The trapping efficiencies were calculated by PISA-QMS as a function of V_{RF}. The injection energy was assumed to be 5 eV. The results obtained for several values of mass between 50u and 1000u are displayed in Fig.5-18. There are specific RF voltages of V_{RF} at which the trapping efficiencies have their respective a maximum. We define these specific RF voltages as $V_{RF}^{(s)}$. The values of $V_{RF}^{(s)}$ are plotted with black circles in Fig.5-19 in accordance with the ion mass.

The results of another calculation of V_{RF} based on the approximation including n=0 and n=±1 modes of oscillations are plotted by open circles in Fig.5-19. The agreement of V_{RF} with $V_{RF}^{(s)}$ is very good. This is the fourth example to show the role of the second and third dominant modes of oscillations on the ion trapping efficiency.

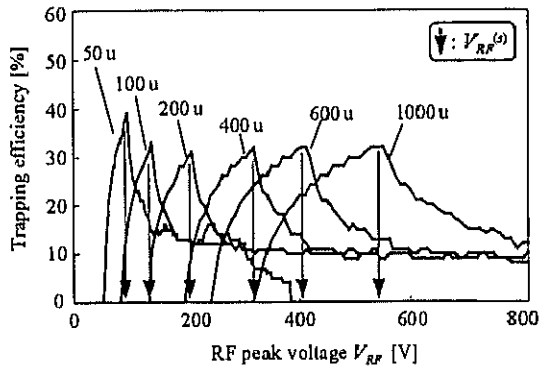

Fig.5-18 The RF peak voltage dependence of the trapping efficiencies obtained by the simulation for 50-1000 u ions when E=5eV. For each ion species there is an optimum injection RF amplitude $V_{RF}^{(s)}$ which gives maximum trapping efficiency.

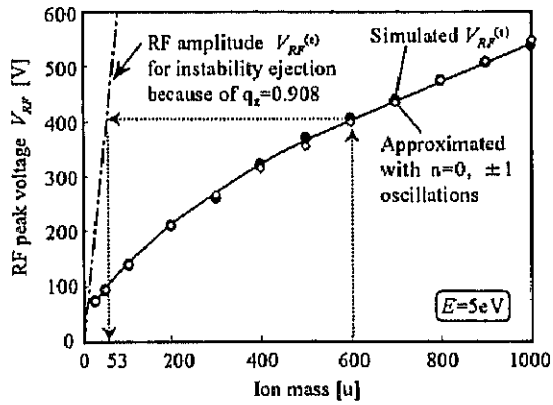

Fig.5-19 Ion mass dependence of the simulated optimum RF peak voltage $V_{RF}^{(s)}$ which gives the maximum trapping efficiency. Open circles are obtained by eqs.(5.2.7) and (5.2.8) when E=5eV. The chain line denotes the RF peak voltage for each ion species to be ejected from ITMS because of ion instability ($q_z \geqq 0.908$).

5.2.6 Proposal of a new injection method

Based on the relationship between the RF voltage $V_R^{(s)}$ and mass of ions represented in Fig.5-19, we proposed a new method for ion injection into ITMS. Instead of the increase of V_{RF} proposed by Doroshenko and Cotter[58], the voltage V_{RF} is decreased during the ion injection period in our method.

In Fig.5-19, the chain line indicates the relation between the mass of ions and the voltages $V_{RF}^{(e)}$ for each ion species to be ejected outside ITMS because of its instability due to q_z>0.908. The value of $V_{RF}^{(s)}$ suitable for the maximum ion trapping of a high mass ion coincides with $V_{RF}^{(e)}$ for lighter mass ions. For example, an RF voltage of 406 V is optimum for trapping of 600u ions,

but ions with mass lower than 53u are ejected outside ITMS. In order to prevent initially trapped ions from being ejected due to the q_z instability, the RF voltage V_{RF} should be decreased. To examine its feasibility, trapping efficiencies were calculated for the following two cases with our program PISA-QMS.

Case 1. The RF voltage V_{RF} was constant during the ion injection period as shown in Fig. 5-20(a). This method is usually employed in current ITMS's.

Case 2. The RF voltage V_{RF} was decreased from the optimum value for trapping 1000u ions to that for 50u ions during the ion injection period. The concept of the variation of V_{RF} is shown in Fig.5-20(b).

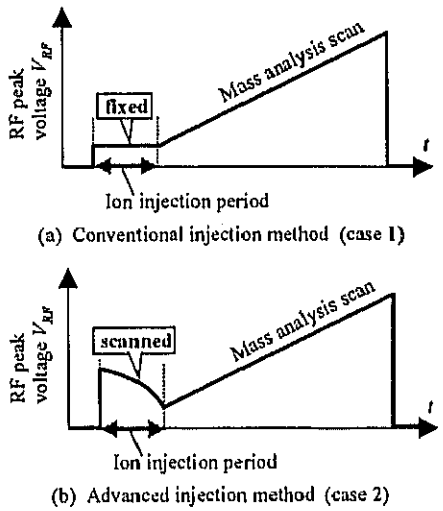

(a) Conventional injection method (case 1)

(b) Advanced injection method (case 2)

Fig.5-20 Two modes of operation of ITMS.

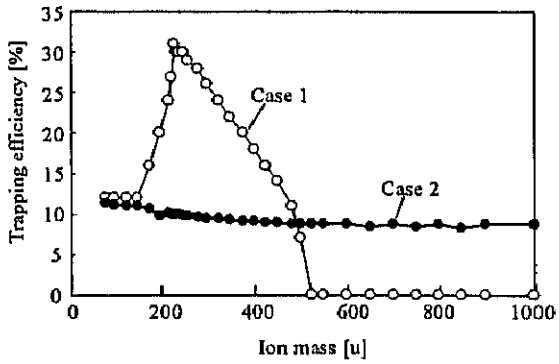

Fig.5-21 The trapping efficiencies simulated in two cases: case 1, conventional injection method in which the RF amplitude V_{RF} was fixed; case 2, advanced injection method in which V_{RF} was decreased.

The results of two simulations are compared in Fig.5-21. The trapping efficiencies in case 1 are large for masses from ~200u to ~400u, but they have strong dependence on the mass. Moreover, no trapping efficiency is realized for the masses heavier than ~500u.

The trapping efficiencies in case 2 are almost flat, around 10 %, over the mass range up to 1000u. The advantage of our method of ion injection is that the relative sensitivity as a mass

spectrometer is almost uniform over a wide mass range. Therefore, our proposed method is very useful to mass analyze unknown substances. This property is valuable for preparing a sensitivity calibration curve also. The decreased absolute value of the trapping efficiency can be compensated with other methods like chemical enrichment. However, if the sample substances are expected to be in a narrow mass range, the optimum values of the RF voltage $V_{RF}^{(s)}$ are also given in a narrow range according to our finding of Fig.5-19. In that case, RF voltage V_{RF} should be fixed at the typical value $V_{RF}^{(s)}$ within the range to obtain higher intensity. Therefore, we propose that mass analysis is performed by the combination of the two injection methods. First, sample is analyzed by our proposed injection method to determine its mass range. Next, the samples, the mass range of which are known then, are analyzed by fixing RF voltage at $V_{RF}^{(s)}$. Thus, the relationship between the ion mass and the optimum RF voltage (in Fig.5-19) can be used as a fundamental formula for mass analysis of a sample to obtain its mass distribution with high intensity.

5.3 Influences of mass scan speed on mass spectra in ITMS

In order to improve the ITMS mass resolution and mass accuracy, various studies and developments have been conducted so far. In the early 1990s, mass resolution was found to be enhanced by slow mass scanning[59,60]. Kaiser *et al.*[59] reported that the mass resolution (FWHM) at 933u and 1781u was approximately doubled when the mass scan speed was reduced from 16,667 [u/s] to 7,692 [u/s] (almost 1/2). Schwartz *et al.*[60] demonstrated that the mass resolution of about 30,000 was achieved with very slow mass scan speed of 27.8 [u/s], that is 1/400-1/200 of the normal one. They also showed that a shifting of the mass peak position, *i.e. mass shift*, occurs with each slow scanning. Georinger *et al.*[61] theoretically derived the relationship between the mass resolution and the scan speed, but mass shift was not considered. On the other hand, slowing the mass scan speed meets with two problems. (1) The total scan time increases enormously. (2) The mass shift occurs as reported by Schwartz *et al.*[60] and Amster[62]. To solve the above problems, we have investigated the influence of the scan speed on the mass resolution and the mass shift degree using PISA-QMS.

5.3.1 Mass peak position

The mass analysis scan for ions in the mass range of m_0- m_1 is schematically shown in Fig.5-22. After injecting ions into ITMS in the period of T_{inj}, ions are selectively excited by resonating with the auxiliary RF electric field as indicated in Subsection 3.3.4. The mass-to-charge ratio of the excited ions is scanned in the period of T_{scan} at a constant scan speed V_{scan} (= $(m_1 - m_0)/T_{scan}$). Actually, mass scan is carried out by changing the magnitude of V_{RF}.

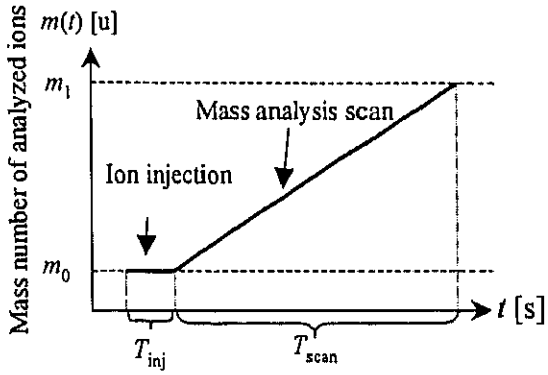

Fig.5-22 Schematic diagram of the mass analysis scan.

Table 5-3 ITMS parameters used to simulate mass spectra.

RF voltage $V_{RF}\cos(\Omega t+\phi)$	
RF frequency $f=\Omega/2\pi$	909kHz
RF amplitude V_{RF}	72.6-4723 V
Mass range	100-500 u
Inner radius of the ring electrode r_0	10mm
Auxiliary RF voltage	
Auxiliary RF frequency (ω_{res})	360kHz
Auxiliary RF amplitude (V_{res})	3V (0-p)
Resonance ejection condition	q_z=0.859 (β_z=0.792)
Helium gas pressure P_{He}	1.0×10^{-4} Torr (1.33×10^{-2} Pa)
Assumed radius of space charge R_s	5mm
Ion density ρ	2.0×10^{6} /cm^3

At first, we calculated the ion trajectories with various mass scan speeds V_{scan} by PISA-QMS. The parameters used for this simulation are shown in Table 5-3. Based on the calculated trajectories of 1620 ions which have different initial conditions, the mass spectra of 100-500u ions were obtained. These simulated mass spectra of 200u ions are shown in Fig.5-23. The shape of the calculated mass peaks was fitted with a Gaussian curve. We confirmed that the mass resolution is enhanced, whereas the mass peak position is shifted to the low mass side as the scan speed is lowered.

The relationship between the scan speed and the mass peak position was investigated from the calculated mass spectra. These results are shown in Fig.5-24. The peak position is approximately

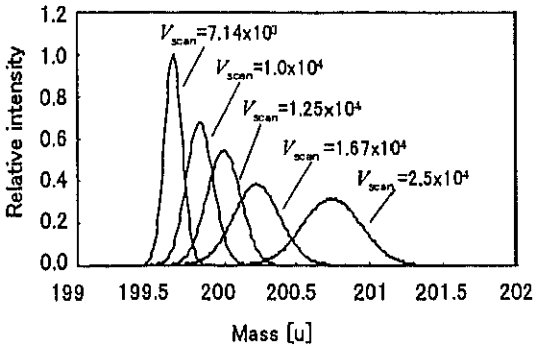

Fig.5-23 Simulated mass spectra of 200 u ions for different scan speeds, V_{scan} [u/s].

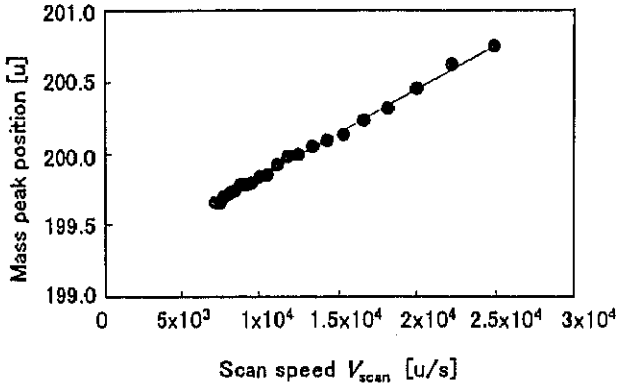

Fig. 5-24 The relationship between the mass peak position and the scan speed for 200 u ions.

proportional to the scan speed V_{scan}. From this result, an approximate equation of the mass peak position m_{ej} [u] can be derived in the following form:

$$m_{ej} = C \cdot V_{scan} + m^* \tag{5.3.1}$$

where C is the slope and m^* is the intercept of the proportional relationship. According to eq.(5.3.1), ions will exit at the mass point m_{ej}. Even when the scan speed V_{scan} is set zero, ions exit at the mass point $m_{ej}=m^*$. This means that ions already begin exciting with the auxiliary RF field at the mass point m^* and they can exit without mass scanning. Therefore, the mass point m^* can be defined as the start point of resonance excitation during the mass scan as shown in Fig.5-25.

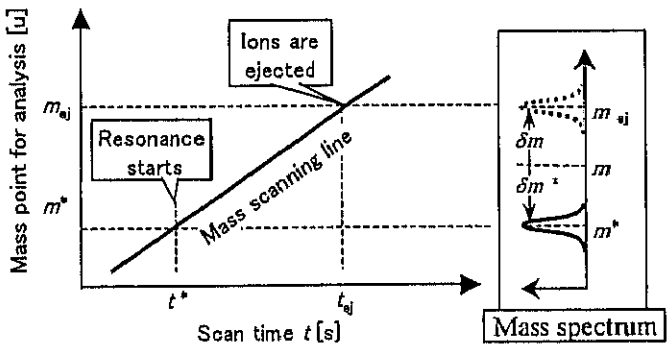

Fig.5-25 Schematic diagram of mass point during mass analysis scan of resonance excitation and ejection for m [u] ions in comparison with the corresponding mass spectrum.

From eq.(5.3.1), the mass shift degree δm is described by

$$\delta m = m_{ej} - m = C \cdot V_{scan} + (m^* - m) = C \cdot V_{scan} + \delta m^* \tag{5.3.2}$$

with the following definition:

$$\delta m^* = m^* - m \tag{5.3.3}$$

where m means the ion's exact mass number. Next, the relationship between the scan speed V_{scan} and the mass shift degree δm, which was obtained by simulation, was investigated for 100, 300 and 500u ions. The results are shown in Fig.5-26. As shown in eq.(5.3.2), the mass shift degree values δm are in proportion to the scan speed V_{scan}, while the proportional slopes, *i.e.* C values in eq.(5.3.2), differ according to the ion masses. The ion mass dependence of the slope C is obtained as shown in Fig.5-27. Since the slope C is proportional to ion mass number m, eq.(5.3.2) can be rewritten as

$$\delta m = m_{ej} - m = C_m \cdot m \cdot V_{scan} + \delta m^* \tag{5.3.4}$$

where C_m is the slope of the relationship between the slope C and the ion mass m ($C_m = C/m$).

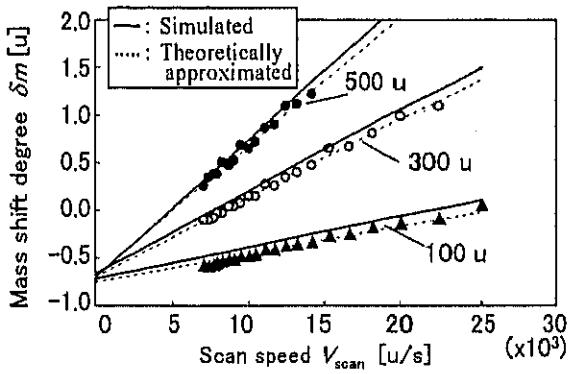

Fig.5-26 The relationship between scan speed V_{scan} and mass shift degree δm.

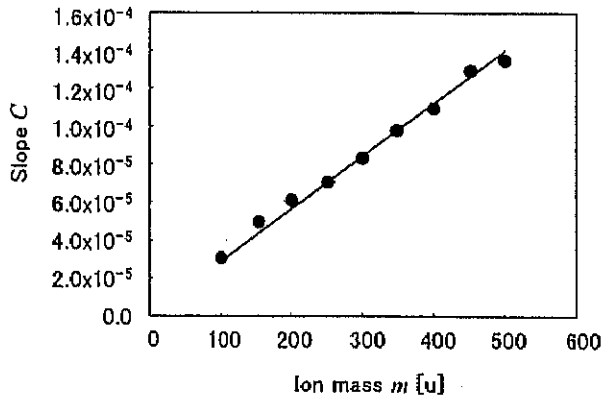

Fig.5-27 The dependence of ion mass m on slope C in eq.(5.3.1).

Thus, from the simulation results, the approximate relation between the mass shift degree δm and the scan speed V_{scan} is obtained in the form of eq.(5.3.4). We attempted to understand this result theoretically as follows.

When the auxiliary RF voltage $V_{res}\sin(\omega_{res}t+\phi_0)$ is applied in dipolar fashion to the end-cap electrodes, the equation of ion motion in z-direction can be described approximately by

$$\ddot{z}+\omega_{z0}{}^2 z=-qE_{res}\approx -q\frac{V_{res}\sin(\omega_{res}t+\phi_0)}{mz_0} \tag{5.3.5}$$

where ω_{z0} is the fundamental angular frequency of ion oscillation in z-direction and z_0 is half of the distance between the two end-cap electrodes. By setting the angular frequency ω_{res} of the auxiliary RF voltage equal to the fundamental one ω_{z0} of ion oscillation, ions start to be excited until they exit from ITMS. The damping force caused by collision with He gas and the interaction with the space charge were not considered in eq.(5.3.5). The excited ion motion is approximately obtained by substituting $\omega_{res}=\omega_{z0}$ and $z=A(t)\cos\omega_{z0}t$ into eq.(5.3.5) as follows:

$$z=A(t)\cos\omega_{z0}t=\left(A_0+\frac{eV_{res}}{mz_0}\frac{1}{2\omega_{z0}}t^*\right)\cos\omega_{z0}t \tag{5.3.6}$$

where t^* is the elapsed time since the resonance excitation has started and A_0 is the amplitude of the ion oscillation when no resonance voltage is applied. According to eq.(5.3.6), the amplitude $A(t)$ increases linearly with the elapsed time t^*. Ions are ejected when the amplitude $A(t)$ can reach the position of the apex of the end-cap electrodes ($A(t)=z_0$). While resonance exciting, the mass number of the excited ions is scanned at the scan speed V_{scan} [u/s]. From eq.(5.3.6), the time needed for resonance ejection since the resonance excitation has begun, is expressed by

$$t_{ej}=2\omega_0\frac{mz_0}{qV_{res}N_A}\cdot(z_0-A_0)=(m_{ej}-m^*)/V_{scan} \tag{5.3.7}$$

where m_{ej} [u] is mass point when ions are actually ejected during the mass scan. Eq.(5.3.7) can be transformed as follows:

$$m_{ej} = 2\omega_{z0} \frac{mz_0}{qV_{res}N_A} \cdot (z_0 - A_0) \cdot V_{scan} + m^*. \tag{5.3.8}$$

Therefore, the mass shift degree δm can be expressed using eq.(5.3.3) as follows:

$$\delta m = m_{ej} - m = 2\omega_{z0} \frac{mz_0}{qV_{res}N_A} \cdot (z_0 - A_0) \cdot V_{scan} + \delta m^*. \tag{5.3.9}$$

We also attempt to derive the equation for the value δm^* in eq.(5.3.9) theoretically as described below.

As was stated previously, m^* denotes the scanning mass point when ions of m [u] start resonance exciting. At the resonance q_z point of q_{res}, ions are ejected by resonance with the resonance field. Therefore, the scanning mass point becomes m^*, the q_z value of the ions of m^* ions is equal to q_{res}. On the other hand, the q_z value of the m ions is lower than the value q_{res} as shown in Fig.5-28.

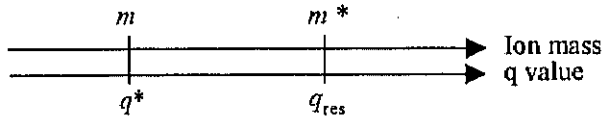

Fig.5-28 Schematic diagram of relationship between mass points m^*, m and q^*, q_{res} values during the mass analysis scan. When ions of m start resonance exciting at mass point m^*, the q_z values of m and m^* are q^* and q_{res}, respectively.

The q_z values of m^* and m ions are expressed using eq.(3.3.14*b*) as

$$q_{res} = \frac{4qV_{RF}N_A}{m^* r_0^2 \Omega^2} \tag{5.3.10}$$

and

$$q^* = \frac{4qV_{RF}N_A}{mr_0^2\Omega^2} = \frac{m^*}{m} q_{res} \tag{5.3.11}$$

where q^* is the q_z value of ions m when the scanning mass point becomes m^* and N_A is Avogadro's number. The difference Δq between q_{res} and q^* is given by

$$\Delta q = q_{res} - q^* = q_{res}(1 - \frac{m^*}{m}) = \frac{q_{res}}{m} \cdot (m - m^*) = -\frac{q_{res}}{m} \cdot \delta m^* . \qquad (5.3.12)$$

We assume that the q_z value difference Δq is determined by the intensity of the resonance field E_{res} (eq.(5.3.5)) relative to the trapping field E_{trap} (eq.(3.3.10)) as follows:

$$\frac{\Delta q}{q_{res}} \approx \frac{E_{res}}{E_{trap}} \qquad (5.3.13)$$

When using the approximations of $\sin(\omega_{res}t+\phi_0)=1$, $\cos\Omega t=1$ and $z=A_0$ with eqs.(5.3.5) and (3.3.10), the resonance field E_{res} and trapping one E_{trap} are approximated in the following forms:

$$E_{res} = |E_{res}| \approx \frac{V_{res}}{z_0} \qquad (5.3.14)$$

and

$$E_{trap} \approx \frac{2V_{RF}}{r_0^2} \cdot A_0 = \frac{q^* A_0 m \Omega^2}{2qN_A} = \frac{q_{res} A_0 \Omega^2 m^*}{2qN_A} . \qquad (5.3.15)$$

From eqs.(5.3.12)-(5.3.15), the value δm^* in eq.(5.3.9) is expressed as follows:

$$\delta m^* = -\frac{E_{res}}{E_{trap}} \cdot m = -\left(\frac{V_{res}}{z_0} \frac{2qN_A}{q_{res} A_0 \Omega^2}\right) \cdot \frac{m}{m^*}$$

$$= -\left(\frac{V_{res}}{z_0} \frac{2qN_A}{q_{res} A_0 \Omega^2}\right) \cdot \frac{m}{(\delta m^* + m)} \qquad (5.3.16)$$

Eq.(5.3.16) is transformed into the following form:

$$\delta m^* \cdot (\delta m^* + m) = -\left(\frac{V_{res}}{z_0} \frac{2qN_A}{q_{res} A_0 \Omega^2}\right) \cdot m . \qquad (5.3.17)$$

With the approximation of $\delta m^* \cdot \delta m^* \approx 0$, the value δm^* can be given by

$$\delta m^* \approx -\frac{V_{res}}{z_0} \frac{2qN_A}{q_{res} A_0 \Omega^2} . \qquad (5.3.18)$$

Therefore, by substituting eq.(5.3.18) into eq.(5.3.9), we obtain the relational expression of the mass shift degree δm theoretically as follows:

$$\delta m = m_{ej} - m = 2\omega_{z0}\frac{mz_0}{qV_{res}N_A}\cdot(z_0 - A_0)\cdot V_{scan} - \frac{V_{res}}{z_0}\frac{2qN_A}{q_{res}A_0\Omega^2}. \qquad (5.3.19)$$

To confirm the accuracy of the relational expression of the mass shift degree, which was derived by a theoretical approximation, the values of δm calculated with eq.(5.3.19) were also plotted in Fig.5-26 (dotted lines) in comparison with the simulated mass shift values. The values of δm calculated with eq.(5.3.19) show good agreement with the simulated ones for 100-500u ions within 0.56 % error. Therefore, the validity of the relational expression in eq.(5.3.19) is verified.

Based on derivation of the theoretical formula of the mass shift degree, the mechanism of the mass shift occurrence is considered. The mass peak position should shift when the time t_{ej} actually needed for ions to be ejected (eq.(5.3.7)) differs from the time t_m needed for ejection at the exact mass point of m. The time t_m is expressed as

$$t_m = (m - m^*)/V_{scan}. \qquad (5.3.20)$$

The supposed mass shifting mechanism is schematically denoted in Fig.5-29. As shown in eq.(5.3.7) the time t_{ej} until ions are ejected is dependent only on the ion masses while the resonance voltage V_{res} is constant. On the other hand, the time t_m (eq.(5.3.20)) is determined only by the mass analysis scan speed V_{scan}. Consequently, our finding suggested that the mass shift occurrence is avoidable by changing the scan speed V_{scan} according to the ion masses m so that the ejection time t_{ej} coincides with the time t_m to avoid the mass shift occurrence.

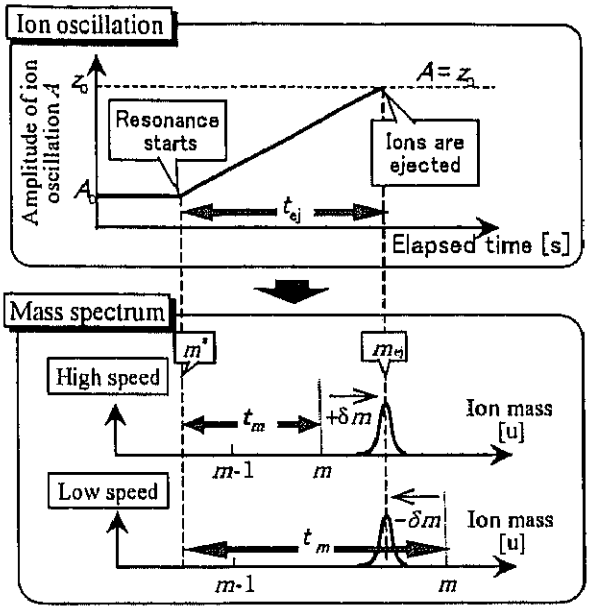

Fig.5-29 Schematic diagram of the mechanism of mass shift occurrence according to the scan speed V_{scan}. The mass peak position should shift when the time t_{ej} needed for resonance ejection differs from the time t_m needed for the mass point to become an accurate mass number m through the mass scan.

5.3.2 Mass resolution

As shown in Fig.5-23, each mass peak has a width which determines the possibility to separate adjacent mass peaks. The smaller the value of the mass peak width Δm becomes, the more the mass resolutions can be enhanced. Therefore, the mass resolution can be evaluated by the mass peak width Δm. From the simulated mass spectra in Fig.5-23, we also obtained the mass peak width Δm. The value of FWHM was employed as the value of the mass peak width Δm. The scan speed versus the value of FWHM, obtained by simulated mass spectra of 100, 300 and 500u ions are plotted in Fig.5-30. The peak width Δm is confirmed to decrease as the scan speed V_{scan} is lowered, although there is some discrepancy. The simulated peak width Δm are approximated by a straight line as expressed in the following form:

$$\Delta m = S \cdot V_{scan} \tag{5.3.21}$$

where S is the ratio of the peak width Δm to the scan speed V_{scan}. The approximated lines of three ion species are denoted by solid lines in Fig.5-30. Kaiser *et al.*[59] also reported that mass resolution was approximately doubled by reducing the scan speed by a half. The ratio S in eq.(5.3.21) is plotted for 100-500u ions in Fig.5-31. As ratio S is also proportional to ion mass m, eq.(5.3.21) can be rewritten as

$$\Delta m = S_m \cdot m \cdot V_{scan} \quad . \tag{5.3.22}$$

where $S_m = S/m$.

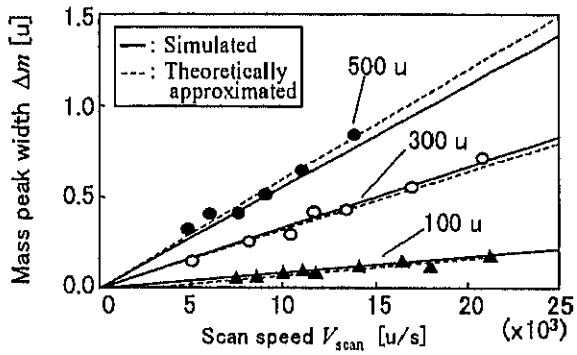

Fig.5-30 The relationship between scan speed V_{scan} and the mass peak width Δm.

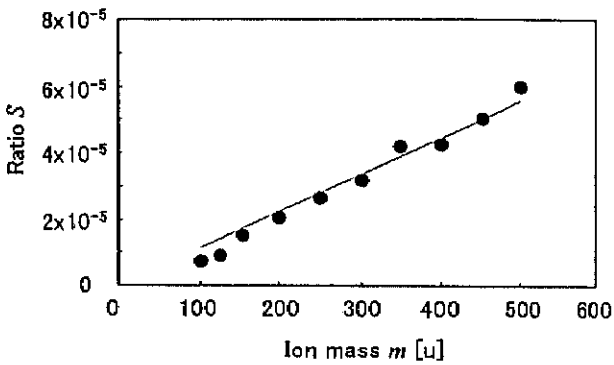

Fig. 5-31 The dependence of ion mass on the ratio S in eq.(5.3.21).

Thus, from the simulation results, the approximate relation between the peak width Δm and the scan speed V_{scan} is obtained in the form of eq.(5.3.22). We considered how to support the above simulation results theoretically as follows.

Ions oscillate at different positions within a certain space even though they are the same ion species due to such reasons as different initial conditions or Coulombic repulsive force. We assume that the value of FWHM is determined by the ejection time difference among ions which are dispersed inside ITMS. When ions of mass number m have the spatial dispersion ΔA, the

relationship between the scan speed V_{scan} and the peak width Δm is derived using Eq.(5.3.8) as follows:

$$\Delta m = 2\omega_0 \frac{mz_0}{qV_{res}N_A} \cdot \Delta A \cdot V_{scan} \quad . \tag{5.3.23}$$

To confirm the accuracy of the relational expression of eq.(5.3.23), derived by theoretical approximation, the values of Δm calculated with eq.(5.3.23) were also plotted in Fig.5-30. The values of Δm calculated with eq.(5.3.23) show good agreement with the simulated ones for 100-500u ions within 0.2 % error. Therefore, the validity of the relational expression in eq.(5.3.23) is also verified.

Based on the above results, the determinant mechanism of the mass resolution is considered. The time period ΔT_i assigned for mass analysis of each ion species is dependent on the scan speed V_{scan}, as expressed in the following form.

$$\Delta T_i = 1/V_{scan} \tag{5.3.24}$$

On the other hand, the difference Δt_i of the ejection time t_{ej} among the dispersed ions should be independent of V_{scan}. The ratio of the ejection time difference to the mass analysis period assigned for each ion species, *i.e.* $\Delta t_i/\Delta T_i$, is changed according to the scan speed V_{scan}. The supposed mechanism determining the mass resolution is schematically indicated in Fig.5-32. The ratio of $\Delta t_i/\Delta T_i$ can be regarded as the peak width Δm. As the scan speed is lowered, the time period ΔT_i for mass analysis of each ion species is prolonged. Therefore, at low scan speed, the ratio of $\Delta t_i/\Delta T_i$, that is Δm, becomes smaller and the mass resolution is enhanced. Based on the relationship of eq.(5.3.23), the scan speed V_{scan} can be determined according to the necessary maximum resolution $m/\Delta m$ for the mass analysis within the ion mass range. However, the conventional mass analysis scan with a constant and low speed causes a scan time expansion and mass shift occurrence as reported by Schwartz *et al.*[60] and Amster[62].

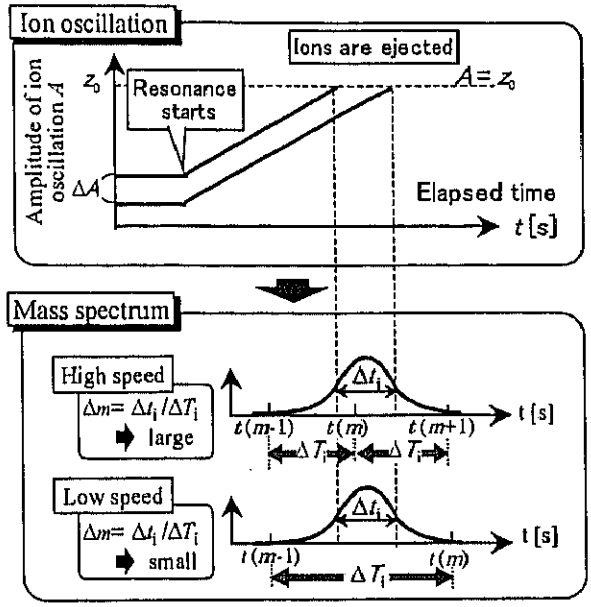

Fig.5-32 Schematic diagram of the mechanism determining the peak width Δm according to the scan speed V_{scan}. The ratio of the ejection time difference to the mass analysis period assigned for each ion species i.e. $\Delta t_i/\Delta T_i$, can be regarded as the mass peak width Δm.

5.3.3 Proposal of a new mass scanning method

In Subsections 5.3.1 and 5.3.2 we obtained the relationships between the mass scan speed V_{scan} and basic performance parameters, mass accuracy and mass resolution by using PISA-QMS. Based on the relationships, we propose a new mass scanning method.

In the conventional scanning method, the mass scan is performed at a constant speed V_{scan}. According to the relationship between the scan speed V_{scan} and the peak width Δm (FWHM) in eq.(5.3.23), the value of Δm increases in proportion to the mass number m in the conventional method. Therefore, the constant scan speed V_{scan} has had to be set very low to obtain a low value of Δm, especially for high mass ions. On the other hand, the peak width Δm of low mass ions becomes excessively low if the scan sped is very slow. In many cases, high mass resolution is not

necessary for low mass ions. If the peak width Δm is kept constant and low enough for all ion species, all mass spectra can be separated adequately while reducing the total scan time. The relationship of eq.(5.3.23) suggests that the scan speed V_{scan} should be controlled in inverse proportion to ion mass m to obtain constant Δm. The time needed for mass analysis of each ion species, $T_i(m)$, can be derived from eq.(5.3.22) as follows:

$$T_i(m) = 1/V_{scan}(m) = S_m \cdot m / \Delta m \tag{5.3.25}$$

where S_m is given by

$$S_m = \frac{2\omega_0 z_0 \Delta A}{q V_{res} N_A} . \tag{5.3.26}$$

The scan time t, that is elapsed while mass scanning from m_0 to m, is obtained by integrating eq.(5.3.25) with ion mass m as shown in the following form:

$$t = \int_{m_0}^{m} (S_m / \Delta m) \cdot m \cdot dm = S_m \cdot (m^2 - m_0^{\,2}) / 2\Delta m . \tag{5.3.27}$$

The ion mass m, being mass analyzed, should be scanned with time according to the following formula:

$$m(t) = \sqrt{\frac{2\Delta m}{S_m} \cdot t + m_0^{\,2}} . \tag{5.3.28}$$

Consequently, in our proposed method, the scan speed V_{scan} is lowered nonlinearly with time as follows:

$$V_{scan} = \frac{dm(t)}{dt} = \cdot \frac{\Delta m}{S_m} \Big/ \sqrt{\frac{2\Delta m}{S_m} \cdot t + m_0^{\,2}} . \tag{5.3.29}$$

Furthermore, by substituting practical ion mass m for m_{ej} (that is δm=0) in eq.(5.3.19), we obtain the formula which causes no mass shift (δm=0) on the mass spectra as follows:

$$2\omega_0 \frac{m z_0}{q V_{res} N_A} \cdot (z_0 - A_0) \cdot V_{scan} - \frac{V_{res}}{z_0} \frac{2qN_A}{q_{res} A_0 \Omega^2} = 0 . \tag{5.3.30}$$

We call eq.(5.3.30) the *formula for no mass shift* in this dissertation. The formula for no mass shift is transformed by eq.(5.3.23) into

$$V_{res} = \frac{(z_0 - A_0) z_0 q_{res} A_0 \Omega^2}{2qN_A \Delta A} \cdot \Delta m \ . \tag{5.3.31}$$

During the mass scan, the constant peak width Δm is obtainable by setting the resonance voltage V_{res} constant so that eq.(5.3.31) is satisfied, while the parameters q_{res}, A_0, Ω and ΔA are assumed to be determined.

Therefore, we proposed a new scanning method in which the scan speed V_{scan} is changed nonlinearly with time as expressed in eq.(5.3.29) and the resonance voltage V_{res} is determined by the formula for no mass shift of eq.(5.3.31). With the new scanning method, the mass peak width Δm should be constantly low enough to separate adjacent ions independently of ion mass without mass shift and scan time expansion.

To examine the effect of the new scanning method based on eqs.(5.3.29) and (5.3.31), the mass spectra of 100-500u ions were simulated. The operating parameters used for these simulations are shown in Table 5-4. In cases 2 and 4 the auxiliary RF voltage V_{res} was determined with eq.(5.3.31) and the mass number of ions to be separated was scanned using eq.(5.3.28), while other cases employed the conventional method in which the mass scan was conducted at a constant speed. Simulations in cases 1 and 5 used the same value of resonance voltage V_{res} as cases 2 and 4, respectively. The constant scan speeds of cases 1 and 5 were obtained by eq.(5.3.23) so that mass resolution of the highest mass ions (500u in this case) would be the same as those of cases 2 and 4. Case 3 also employed the conventional scan so that the total scan time became almost the same as that of case 2. The scanning manner adopted for cases 1-3 is indicated in Fig.5-33.

Table 5-4

Parameters used for the simulations of mass spectra in cases 1-5.

	Case 1	Case 2	Case 3	Case 4	Case 5
Amplitude of auxiliary RF voltage V_{res} [V]	2.14	2.14	3.0	1.43	1.43
Scan speed [u/s]	3876	Varied with time*	7140	Varied with time*	1724
Total scan time [ms] (mass range: 10-500u)	126	64.5	68.6	145	284

*: The scan speed is varied nonlinearly with time based on formula (5.3.29).

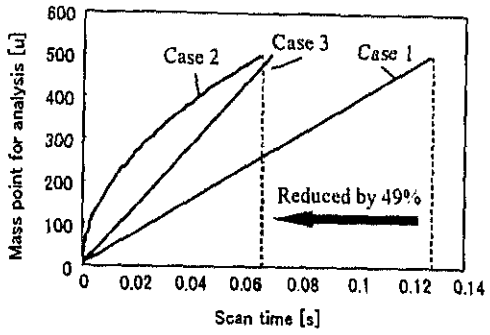

Fig.5-33 The scanning method of mass analysis used for the simulations of cases 1-3.

The peak width (FWHM) Δm obtained from these simulations is shown in Fig.5-34. In cases 2 and 4, the values of peak width Δm are constant for all ion species at low values of 0.2 and 0.07u, respectively. As predicted from eq.(5.3.21), the peak widths Δm of 500u ions in cases 1 and 5 are almost the same as those of cases 2 and 4, respectively. However, the total scanning time in case 2 is shorter than that of case 1 by 49% as shown in Fig.5-33. In case 1, the peak widths decrease as the ion masses become lower. When high resolution is not necessary for such low mass ions, slow scanning for low mass ions could be a waste of time. Next, the peak widths of cases 2 and 3 are compared. Although the total scanning time in case 3 is almost the same as that in case 2, the mass resolution in case 3 is much lower than that for case 2. For example, the peak width value Δm of 500u ions in case 3 is almost three times of that of case 2. Therefore, the proposed scanning method is verified to reduce the total scanning time while maintaining high resolution for high mass ions.

The mass shift degrees δm obtained from these simulations are shown in Fig.5-35. The mass shifts in cases 1, 3 and 5 depend differently on ion masses m. In cases 2 and 4, the mass shift degrees δm are kept constantly low for all ion species, although they are all shifted slightly by 0.07-0.1u. This slight shift is thought to be caused by using approximate formulas, eqs.(5.3.29) and (5.3.31), to calculate the scan speed and the resonance voltage. However, this slight shift can

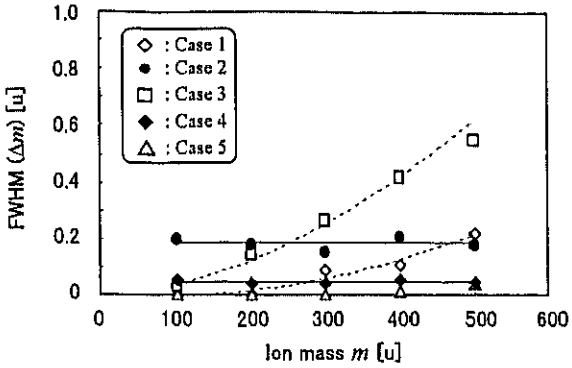

Fig.5-34 The dependence of ion mass m on the value of FWHM Δm obtained in the simulations of cases 1-5.

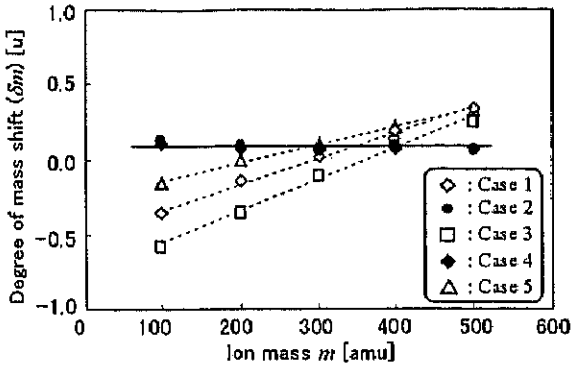

Fig.5-35 The dependence of ion mass m on the mass shift degree δm obtained in the simulations of cases 1-5.

be easily compensated because it is constant and independent of both the ion mass m and the auxiliary RF voltage V_{res}.

The demonstrated validity of the proposed scanning method, in which the scan speed is controlled based on formulas (5.3.29) and (5.3.31), shows that mass spectra can be given with high resolution and high accuracy in a shortened scanning time.